Data-driven Optimal Scheduling of Isolated Microgrid Using Random Forest Regressor

Data-driven Optimal Scheduling of Isolated Microgrid Using Random Forest Regressor

Seyed Farhad Zandrazavi
School of Technology and Innovations
University of Vaasa
Vaasa, Finland
seyed.zandrazavi@uwasa.fi

Miadreza Shafie-khah
School of Technology and Innovations
University of Vaasa
Vaasa, Finland
mshafiek@uwasa.fi

Meysam Pashaei
School of Technology and Innovations
University of Vaasa
Vaasa, Finland
meysam.pashaei@uwasa.fi

***Abstract*— Design, operation, and planning of Microgrids (MGs) have been enriched by advances in machine learning (ML) techniques and availability of real data. These advancements have significantly improved the accuracy of predictions related to energy demand and renewable generation within MGs. ML-based algorithms can analyze complex patterns in data to make precise forecasts about future energy demands, renewable energy output, and even potential system failures. In this context, this paper utilizes real open-access wind speed dataset from Nottingham to create a forecast model based on a random forest regressor (RFR). This forecasted data, along with actual wind speed for wind power generation, serves as the input for a mixed-integer linear programming model designed for the optimal scheduling of standalone microgrids (OSSM). The results demonstrate that the discrepancies in the total cost, voltage deviation, and power loss of the MG, when comparing forecasted data to actual data, are less than 5%, 1%, and 2%, respectively. These results validate the effectiveness of ML-based models, specifically RFR, in the development of OSSM.**

Keywords*— Data-driven, forecast, machine learning, random forest regressor, standalone microgrids.

NOMENCLATURE

Acronyms	
DER	Distributed energy resource
DG	Dispatchable distributed generation unit
ESS	Energy storage system
MG	Microgrid
MILP	Mixed-integer linear programming
ML	Machine learning
OF	Objective function
OSSM	Optimal scheduling of standalone microgrid
PL	Power loss
PV	Photovoltaic
RFR	Random forest regressor
RMSE	Root mean square error
VD	Voltage deviation
Indices	
k, b, n	Index for buses
$\boldsymbol{bn}$,	Index for lines
$\boldsymbol{t}$	Index for time period
$\boldsymbol{dg}$	Index for distributed generation units
$\boldsymbol{ess}$	Index for energy storage systems
$\boldsymbol{wu}$	Index for wind turbine units
$\boldsymbol{\omega}$	Index for pieces in piecewise linearization
Parameters	
$\boldsymbol{V^{WU}}$	Wind speed
$\boldsymbol{V_{ci}^{WU}}$	Cut-in speed
$\boldsymbol{V_{no}^{WU}}$	Nominal speed
$\boldsymbol{V_{co}^{WU}}$	Cut-out speed
$\boldsymbol{P_{no}^{WU}}$	Nominal capacity of the wind turbine
$\boldsymbol{\alpha_{dg}, \beta_{dg}, \gamma_{dg}}$	Coefficients associated with DGs' operation cost
$\boldsymbol{\Delta_t}$	Time period
$\boldsymbol{\Psi_{n,t}^{ENS}}$	Cost of energy not supplied
$\boldsymbol{R_{bn}, X_{bn}, Z_{bn}}$	Resistance, reactance, & impedance of lines
$\boldsymbol{P_{b,t}^{L}, Q_{b,t}^{L}}$	Active & reactive power demand
$\boldsymbol{P_{wu,t}^{WU}}$	Power generation of wind turbine
$\boldsymbol{V^{min}, V^{max}}$	Minimum & maximum voltages
$\boldsymbol{I^{max}}$	Maximum current
$\boldsymbol{P_{dg}^{min}, P_{dg}^{max}}$	Minimum & maximum DGs' active power
$\boldsymbol{\varphi_{dg}}$	Angle between active & apparent power in DGs
$\boldsymbol{P_{ess}^{max}}$	Maximum power of ESSs
$\boldsymbol{\eta_{ess}^{Ch}, \eta_{ess}^{Dis}}$	Charging & discharging efficiency of ESSs
$\boldsymbol{\beta_{ess}}$	Self-discharge rate of ESSs
$\boldsymbol{\ddot{E}_{ess}^{ESS}}$	Initial energy stored in ESSs
$\boldsymbol{E_{ess}^{min}, E_{ess}^{max}}$	Minimum & maximum energy stored in ESSs
$\boldsymbol{e_{ess,t}}$	Energy stored in ESSs
$\boldsymbol{V_{b,t}^{est}}$	Estimated square of voltages
$\boldsymbol{m_{dg,\omega}^{DG}}$	Slope of blocks in linearization of power in DGs
$\boldsymbol{m_{bn,\omega}^{PQ}}$	Slope of blocks in linearization of power in lines
$\boldsymbol{\Delta P_{dg}^{max}}$	Maximum discretization blocks of power in DGs
$\boldsymbol{\Delta S_{bn}^{max}}$	Maximum discretization blocks of power in lines
$\boldsymbol{\overline{\omega}}$	Number of pieces in piecewise linearization
Variables	
$\boldsymbol{p_{dg,t}^{DG}, q_{dg,t}^{DG}}$	Active & reactive power of DGs
$\boldsymbol{p_{bn,t}, q_{bn,t}}$	Active & reactive power flowing in lines
$\boldsymbol{\omega_{dg,t}}$	Binary variable associated with DGs' commitment
$\boldsymbol{v_{b,t}^{sqr}, i_{bn,t}^{sqr}}$	Square of voltage & current
$\boldsymbol{p_{ess,t}^{ESS}}$	Active power of ESS
$\boldsymbol{p_{ess,t}^{ESS+}, p_{ess,t}^{ESS-}}$	Charging & discharging power of ESSs
$\boldsymbol{\sigma_{ess,t}^{+}, \sigma_{ess,t}^{-}}$	Binary variable associated with ESSs
$\boldsymbol{\Delta p_{dg,t,\omega}^{DG}}$	Discretization blocks of active power in DGs
$\boldsymbol{\Delta p_{kb,t,\omega}, \Delta q_{kb,t,\omega}}$	Discretization blocks of power flowing in lines
$\boldsymbol{p_{bn,t}^{+}, q_{bn,t}^{+}}$	Active & reactive power in line (positive direction)
$\boldsymbol{p_{bn,t}^{-}, q_{bn,t}^{-}}$	Active & reactive power in line (negative direction)
$\boldsymbol{p_{t}^{Loss}}$	Power loss
$\boldsymbol{VD_t}$	Voltage deviation

This research was supported by the Horizon Europe project DiTArtIS, grant agreement number: 101079242. Seyed Farhad Zandrazavi also acknowledges Finnish Cultural Foundation for grant 00241288 Central Fund.

I. INTRODUCTION

The swift progress in renewable energy technologies, coupled with declining costs, offers significant socio-economic advantages, particularly for developing countries, in transitioning to 100% renewable energy systems by 2050. This shift underscores the worldwide benefits, including mitigating climate change, enhancing energy security, and promoting sustainable development through the adoption of renewable energy [1]. To achieve this objective, microgrids (MGs) are crucial in enabling the integration of distributed energy resources (DERs), including wind turbine units (WUs), photovoltaics (PVs), and energy storage systems (ESSs). These technologies are essential for creating more

flexible and resilient energy infrastructures that can adapt to varying energy demands and supply sources [2].

A. Motivation

The intermittency of renewable energy generation, characterized by fluctuations in wind speed and solar radiation , poses significant challenges for the reliable operation and efficient scheduling of MGs [3]. This variability can lead to complications in balancing supply and demand, necessitating advanced strategies to mitigate its adverse impacts. However, by harnessing historical datasets and deploying machine learning (ML), it becomes feasible to develop sophisticated forecasting models capable of predicting short-term renewable energy outputs with remarkable accuracy [4]. These forecasts enable the precise modeling of day-ahead scheduling for MGs, allowing operators to optimize energy resources, minimize operational costs, and ensure stability. This approach not only addresses the challenges posed by intermittency but also unlocks the potential for more sustainable and reliable energy management within MGs.

B. Literature

Numerous review articles explored the applications of ML in power system in general [5] and in MG specifically [6]. Here some of the recent works where used ML techniques in the optimal scheduling of MGs are reviewed. In [7], adaptive network-based fuzzy inference system alongside a hybrid metaheuristic algorithm is used for data forecasting to handle uncertainties related to load, energy prices, and renewable generation in MGs. To address the challenges of PV generation variability due to unpredictable solar irradiance, a recurrent neural network for accurate forecasting of solar irradiance and cloud cover is reported in [8], enabling more efficient operation based on weather conditions. A multilayer hybrid forecasting model is employed in [9] to predict wind power generation and load aiming to minimize operational costs while embracing uncertainties. In [10], two types of forecast data are defined: day-ahead and ultra-short-term, both of them serve as the foundation for developing a dynamic robust optimization model that copes with the complexities of MG energy management over multiple time scales. Despite precious contributions, previous studies primarily focus on improving forecast accuracy measured by metrics like root mean square error (RMSE). However, there is a noticeable absence of comprehensive analysis on how these improved forecasts translate to operational performance in the optimal scheduling of MGs.

C. Contribution

As mentioned, different ML techniques have been used in the literature to address the optimal scheduling of MGs. However, it is useful to compare some indices such as total cost, power loss (PL), and voltage deviation (VD) to evaluate the effects of an accurate forecast not only based on RMSE, but also on the final operation of MGs.

In conclusion, the contributions of this research are summarized as follows:

- Utilizing random forest regressor for forecasting wind speed and wind power generation using freely available real-world dataset from Nottingham.
- Developing a nonlinear model for the optimal scheduling of standalone microgrids (OSSM) and then extracting the linearized model by utilizing piecewise linearization and approximation.
- Validating the effectiveness of the proposed model in OSSM by comparing the total cost, PL, and VD between actual and forecasted renewable generation.

II. Methodology

In this section of the paper, firstly the framework for the data-drive optimal operation of standalone MGs by combining data forecast and mathematical optimization is presented. Subsequently, a precise non-linear, non-convex model for the OSSMs is presented. Finally, this model is linearized to ensure both the tractability of the optimization model and the optimality of the solutions. In Fig. 1, the flowchart of the proposed framework for data-driven OSSM is depicted. It can be seen that utilizing real historical data along with an ML-based algorithm known as random forest regressor (RFR) enables the extraction of a day-ahead forecast for wind speed. Subsequently, both the forecasted and actual wind speed data are employed to determine the corresponding wind power generation, taking into account the wind speed and the specific characteristics of the wind turbines. Following this, the actual and predicted WU generation data serve as inputs for the mixed-integer linear programming (MILP) optimization problem. The following subsections provide a thorough explanation of the key concepts involved.

A. Random Forest Regressor and Wind Speed Forecast

RFR operates as a meta estimator by constructing multiple decision tree regressors on different subsets of the dataset. RFR excels in predicting continuous values for a wide range of applications, thanks to its capability to handle large, complex datasets with non-linear relationships and high dimensionality. It mitigates overfitting by averaging multiple trees' predictions and effectively manages missing data and categorical variables, making it a robust choice for accurate predictions in multifaceted data scenario [11]. Additionally, it is worth noting that the RFR-based forecasting model is developed using the Python programming language [12], leveraging the scikit-learn library [13].

B. Wind Power Generation

The power output of wind turbine units can be determined based on wind speed using (1) [14]. In this paper, V_{ci}^{WU}, V_{no}^{WU}, and V_{co}^{WU} for 1.5 MW WU are considered, 3.5 m/s, 12 m/s, and 25 m/s, respectively [15].

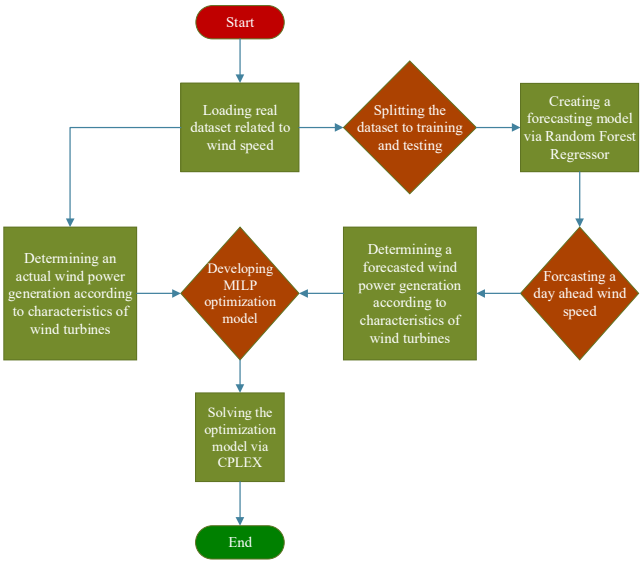

Fig. 1. Flowchart of the proposed data-driven OSSM

$$P^{WU}=\begin{cases}0 \;\; if \;\; V_{co}^{WU}<V^{WU} \;\; or \;\; V^{WU}<V_{ci}^{WU}\\ P_{no}^{WU}\left(\dfrac{(V^{WU})^2-(V_{ci}^{WU})^2}{(V_{no}^{WT})^2-(V_{ci}^{WU})^2}\right) \;\; if \; V_{ci}^{WU}<V^{WU}\le V_{no}^{WU}\\ P_{no}^{WU} \;\; if \;\; V_{no}^{WU}<V^{WU}\le V_{co}^{WU}\end{cases} \quad (1)$$

C. Nonlinear Nonconvex Model of OSSM

In this paper, the objective function (OF) chosen focuses on minimizing the total cost. Equation (2) introduces this nonlinear OF, which consists of both the cost of generating power from dispatchable DGs and the cost associated with energy that is not supplied by the MG.

$$Min\left(\sum_{dg\in DG}\sum_{t\in T}\left(\alpha_{dg}\omega_{dg,t}+\beta_{dg}p_{dg,t}^{DG}\Delta_t+\gamma_{dg}\left(p_{dg,t}^{DG}\right)^2\Delta_t^2\right)+\sum_{n\in N}\sum_{t\in T}\Psi_{n,t}^{ENS}p_{n,t}^{ENS}\Delta_t\right) \quad (2)$$

Bidirectional nonlinear nonconvex AC power flow formula for standalone MGs is presented in (3)–(17) [16]. Constraints (3) and (4) ensure the power balance in the MG and (5) and (6) represent the relationship between power, voltage and current. To guarantee the secure operation, limits linked to voltage and current are modeled in (7) and (8) by imposing specific range. Constraint (9) and (10) address the technical restrictions of DGs' power generation. Charging and discharging of ESSs are modeled in (11)–(17).

$$\sum_{kb}p_{kb,t}-\sum_{bn}\left(p_{bn,t}+R_{bn}i_{bn,t}^2\right)+\sum_{wu|b_{wu}=b}P_{wu,t}^{WU}+\sum_{dg|b_{dg}=b}p_{dg,t}^{DG}=P_{b,t}^{L}-p_{b,t}^{ENS}+\sum_{ess|b_{ess}=b}p_{ess,t}^{ESS};\;\;\forall b,t \quad (3)$$

$$\sum_{kb}q_{kb,t}-\sum_{bn}\left(q_{bn,t}+X_{bn}i_{bn,t}^2\right)+\sum_{dg|b_{dg}=b}q_{dg,t}^{DG}=Q_{n,t}^{L};\;\;\forall b,t \quad (4)$$

$$v_{k,t}^2-v_{b,t}^2=2\left(p_{kb,t}R_{kb}+q_{kb,t}X_{kb}\right)+i_{kb,t}^2Z_{kb}^2;\;\;\forall kb,t \quad (5)$$

$$v_{b,t}^2i_{kb,t}^2=\left(p_{kb,t}^2+q_{kb,t}^2\right);\;\;\forall kb,t \quad (6)$$

$$(V^{min})^2\le v_{b,t}^2\le(V^{max})^2;\;\;\forall b,t \quad (7)$$

$$0\le i_{kb,t}^2\le(I^{max})^2;\;\;\forall kb,t \quad (8)$$

$$P_{dg}^{min}\omega_{dg,t}\le p_{dg,t}^{DG}\le P_{dg}^{max}\omega_{dg,t};\;\;\forall dg,t \quad (9)$$

$$-p_{dg,t}^{DG}\tan\left(\cos^{-1}\left(\varphi_{dg}\right)\right)\le q_{dg,t}^{DG}\le p_{dg,t}^{DG}\tan\left(\cos^{-1}\left(\varphi_{dg}\right)\right);\;\;\forall dg,t \quad (10)$$

$$0\le p_{ess,t}^{ESS+}\le P_{ess}^{max}\sigma_{ess,t}^{+};\;\;\forall ess,t \quad (11)$$

$$0\le p_{ess,t}^{ESS-}\le P_{ess}^{max}\sigma_{ess,t}^{-};\;\;\forall ess,t \quad (12)$$

$$\sigma_{ess,t}^{+}+\sigma_{ess,t}^{-}\le 1;\;\;\forall ess,t \quad (13)$$

$$p_{ess,t}^{ESS}=p_{ess,t}^{ESS+}-p_{ess,t}^{ESS-};\;\;\forall ess,t \quad (14)$$

$$e_{ess,t}^{ESS}=\ddot{E}_{ess}^{ESS}+\Delta_t\left(p_{ess,t}^{ESS+}\eta_{ess}^{Ch}-p_{ess,t}^{ESS-}/\eta_{ess}^{Dis}-e_{ess,t}^{ESS}\beta_{ess}\right);\;\;\forall ess,t|t=1 \quad (15)$$

$$e_{ess,t}^{ESS}=e_{ess,t-1}^{ESS}+\Delta_t\left(p_{ess,t}^{ESS+}\eta_{ess}^{Ch}-p_{ess,t}^{ESS-}/\eta_{ess}^{Dis}-e_{ess,t}^{ESS}\beta_{ess}\right);\;\;\forall ess,t|t\ge 1 \quad (16)$$

$$E_{ess}^{min}\le e_{ess,t}\le E_{ess}^{max};\;\;\forall ess,t \quad (17)$$

D. Linearization

Nonconvex nonlinear optimization problems frequently offer precise representations of real-world scenarios. Nonetheless, the complexity of computations and the lack of guarantees for optimal solutions typically lead to the simplification of these models through linearization. Consequently, methods such as piecewise linearization and approximations are employed to develop the corresponding mixed-integer linear programming (MILP) model. As v_{bt} and $i_{bn,t}$ have not appeared directly in the optimization model, it is possible to substitute $v_{b,t}^2$ and $i_{bn,t}^2$ by new variables $v_{b,t}^{sqr}$ and $i_{bn,t}^{sqr}$. In addition, $v_{b,t}^2$ in the left-hand side of equation (6) can be approximated by $v_{b,t}^{est}$ as presented in (18).

$$V_{b,t}^{est}=\left(\left(V^{max}\right)^2+\left(V^{min}\right)^2\right)/2;\;\forall n,t \quad (18)$$

Variables $p_{kb,t}^2$ and $q_{kb,t}^2$ in the right-hand side of (5) as well as $\left(p_{dg,t}^{DG}\right)^2$ in OF can be linearized deploying piecewise linearization. Therefore,(2)–(17) can be replaced by (19)–(46) to obtain MILP model.

$$Min\left(\sum_{dg\in DG}\sum_{t\in T}\left(\alpha_{dg}\omega_{dg,t}+\beta_{dg}p_{dg,t}^{DG}\Delta_t+\gamma_{dg}\Delta_t^2\sum_{\omega}\left(\left(m_{dg,\omega}^{DG}\Delta p_{dg,t,\omega}^{DG}\right)\right)\right)+\sum_{n\in N}\sum_{t\in T}\Psi_{n,t}^{ENS}p_{n,t}^{ENS}\Delta_t\right) \quad (19)$$

$$\sum_{kb}p_{kb,t}-\sum_{bn}\left(p_{bn,t}+R_{bn}i_{bn,t}^{sqr}\right)+\sum_{wt|b_{wt}=b}P_{wt,t}^{WT}+\sum_{dg|b_{dg}=b}p_{dg,t}^{DG}=P_{n,t}^{L}-p_{n,t}^{ENS}+\sum_{ess|b_{ess}=b}p_{ess,t}^{ESS};\;\;\forall b,t \quad (20)$$

$$\sum_{kb}q_{kb,t}-\sum_{bn}\left(q_{bn,t}+X_{bn}i_{bn,t}^{sqr}\right)+\sum_{dg|b_{dg}=b}q_{dg,t}^{DG}=Q_{n,t}^{L};\;\;\forall b,t \quad (21)$$

$$v_{k,t}^{sqr}-v_{b,t}^{sqr}=2\left(p_{kb,t}R_{kb}+q_{kb,t}X_{kb}\right)+i_{kb,t}^{sqr}Z_{kb}^2;\;\;\forall kb,t \quad (22)$$

$$V_{b,t}^{est}i_{kb,t}^{sqr}=\sum_{\omega}m_{kb,\omega}^{PQ}\left(\Delta p_{kb,t,\omega}+\Delta q_{kb,t,\omega}\right);\;\;\forall kb,t \quad (23)$$

$$(V^{min})^2\le v_{b,t}^{sqr}\le(V^{max})^2;\;\;\forall b,t \quad (24)$$

$$0\le i_{kb,t}^{sqr}\le(I_{kb}^{max})^2;\;\;\forall kb,t \quad (25)$$

$$P_{dg}^{min}\omega_{dg,t}\le p_{dg,t}^{DG}\le P_{dg}^{max}\omega_{dg,t};\;\;\forall dg,t \quad (26)$$

$$-p_{dg,t}^{DG}\tan\left(\cos^{-1}\left(\varphi_{dg}\right)\right)\le q_{dg,t}^{DG}\le p_{dg,t}^{DG}\tan\left(\cos^{-1}\left(\varphi_{dg}\right)\right);\;\;\forall dg,t \quad (27)$$

$$0\le p_{ess,t}^{ESS+}\le P_{ess}^{max}\sigma_{ess,t}^{+};\;\;\forall ess,t \quad (28)$$

$$0\le p_{ess,t}^{ESS-}\le P_{ess}^{max}\sigma_{ess,t}^{-};\;\;\forall ess,t \quad (29)$$

$$\sigma_{ess,t}^{+}+\sigma_{ess,t}^{-}\le 1;\;\;\forall ess,t \quad (30)$$

$$p_{ess,t}^{ESS}=p_{ess,t}^{ESS+}-p_{ess,t}^{ESS-};\;\;\forall ess,t \quad (31)$$

$$e_{ess,t}^{ESS}=\ddot{E}_{ess}^{ESS}+\Delta_t\left(p_{ess,t}^{ESS+}\eta_{ess}^{Ch}-p_{ess,t}^{ESS-}/\eta_{ess}^{Dis}-e_{ess,t}^{ESS}\beta_{ess}\right);\;\;\forall ess,t|t=1 \quad (32)$$

$$e_{ess,t}^{ESS}=e_{ess,t-1}^{ESS}+\Delta_t\left(p_{ess,t}^{ESS+}\eta_{ess}^{Ch}-p_{ess,t}^{ESS-}/\eta_{ess}^{Dis}-e_{ess,t}^{BS}\beta_{ess}\right);\;\;\forall ess,t|t\ge 1 \quad (33)$$

$$E_{ess}^{min}\le e_{ess,t}\le E_{ess}^{max};\;\;\forall ess,t \quad (34)$$

$$p_{dg,t}^{DG}=\sum_{\omega}\Delta p_{dg,t,\omega}^{DG}+P_{dg}^{min}\omega_{dg,t};\;\;\forall dg,t \quad (35)$$

$$\Delta p_{dg,t,\omega}^{DG}\le\Delta P_{dg}^{max};\;\;\forall dg,t,\omega \quad (36)$$

$$\Delta P_{dg}^{max} = \left(P_{dg}^{max} - P_{dg}^{min}\right)/\overline{\omega};\ \forall dg \tag{37}$$

$$m_{dg,t}^{DG} = (2\omega - 1)\Delta P_{dg}^{max};\ \forall dg, \omega \tag{38}$$

$$p_{bn,t} = p_{bn,t}^{+} - p_{bn,t}^{-};\ \forall bn, t \tag{39}$$

$$q_{bn,t} = q_{bn,t}^{+} - q_{bn,t}^{-};\ \forall bn, t \tag{40}$$

$$\sum_{\omega}\left(\Delta p_{bn,t,\omega}\right) = p_{bn,t}^{+} + p_{bn,t}^{-};\ \forall bn, t \tag{41}$$

$$\sum_{\omega}\left(\Delta q_{bn,t,\omega}\right) = q_{bn,t}^{+} + q_{bn,t}^{-};\ \forall bn, t \tag{42}$$

$$\Delta p_{bn,t,\omega} \le \Delta S_{bn}^{max};\ \forall bn, t, \omega \tag{43}$$

$$\Delta q_{bn,t,\omega} \le \Delta S_{bn}^{max};\ \forall bn, t, \omega \tag{44}$$

$$\Delta S_{bn}^{max} = \left(V^{max} I_{kb}^{max}\right)/\overline{\omega};\ \forall bn \tag{45}$$

$$m_{bn,\omega}^{PQ} = (2\omega - 1)\Delta S_{bn}^{max};\ \forall bn, \omega \tag{46}$$

E. Power Loss and Voltage Deviation Indices

After solving the optimization model, p_t^{Loss} which is an index showing the active power loss of the lines of MGs and VD_t which is an index indicating the properness of voltage profile in MGs can be calculated based on (47) and (48), respectively.

$$p_t^{Loss} = \sum_{bn} R_{bn} i_{bn,t}^{sqr};\ \forall t \tag{47}$$

$$VD_t = \sum_{b}\left(\sqrt{v_{b,t}^{sqr}} - V^{ref}\right)^2;\ \forall t \tag{48}$$

III. Results and Discussion

The actual wind speed data which is measured every 5 minutes from June 1, 2020, to May 31, 2021 in Nottingham [17] has been used as input data for RFR. The comparison between actual wind speed and forecasted one for both training and testing data sets are shown in Fig. 2 and Fig. 3. It is worth mentioning that 80% of data used for training and 20% used for testing. Moreover, actual and forecasted wind speed for 24 hours is depicted in Fig. 4. To validate the proposed data-driven OSSM using RFR, a modified 33-bus network consisting of WUs, ESSs, and DGs, is considered as illustrated in Fig. 5. The data of this test system is presented in Table I and Table II. It is noteworthy that the optimization model has been developed in AMPL IDE [18] and solved by CPLEX [19]. The profile of active and reactive power demand are shown in Fig. 6 and are identical to those detailed in [20].

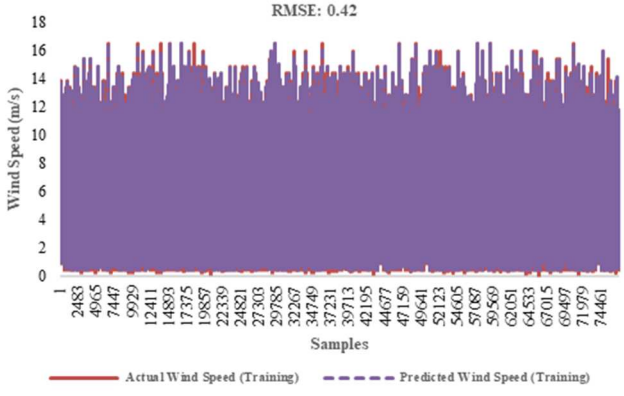

Fig. 2. Actual vs. Predicted wind speed in training data

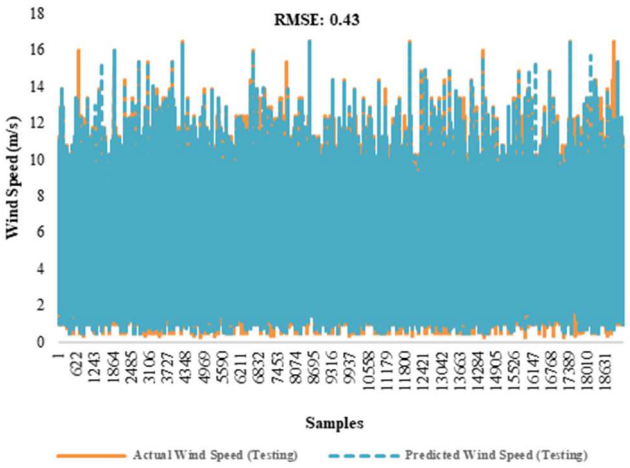

Fig. 3. Actual vs. Predicted wind speed in testing data

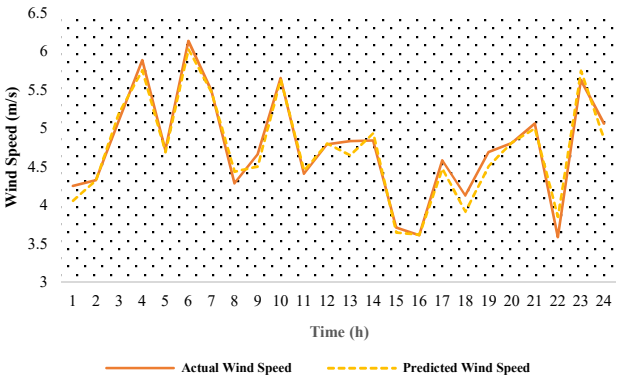

Fig. 4. Actual vs. Predicted wind speed for 24 hours

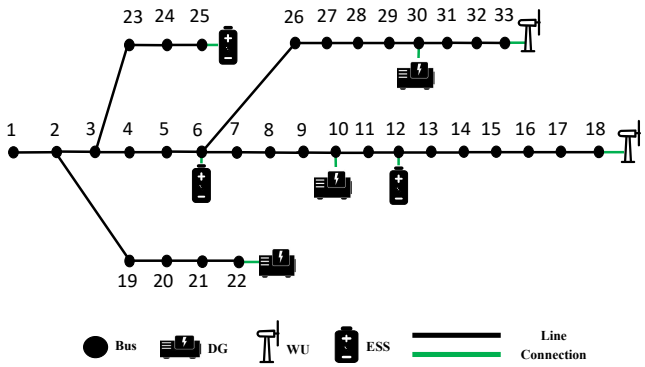

Fig. 5. Standalone 33-bus microgrid

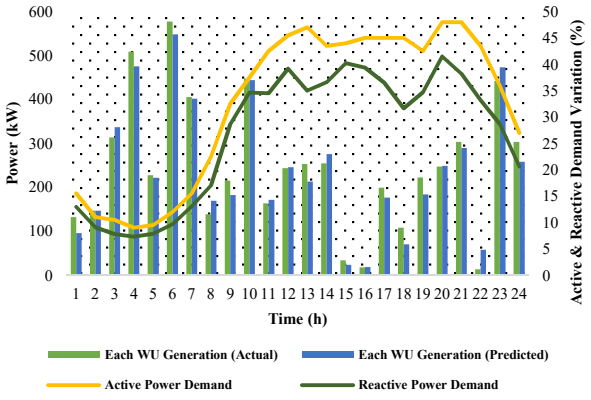

Fig. 6. Actual and predicted generation of WU and profile of power demand

TABLE I. DATA ON DG

Parameter	DG 1	DG 2	DG 3
Bus	10	22	30
P_{dg}^{max}(kW)	500	500	1000
P_{dg}^{min}(kW)	50	50	100
φ_{dg}	0.8	0.8	0.8
α_{dg}($)	27	25	26
β_{dg}($/MWh)	85	90	83
γ_{dg}($/MWh^2)	0.003	0.003	0.170

TABLE II. DATA ON ESS

Parameter	ESS 1	ESS 2	ESS 3
Bus	6	12	25
P_{ess}^{max}(kW)	200	200	100
E_{ess}^{max}(kWh)	1000	1000	500
E_{ess}^{min}(kWh)	100	100	50
η_{ess}^{Ch} & η_{ess}^{Dis}	0.80	0.80	0.85
β_{ess}	0.002	0.001	0.004

A. Scheduling of DGs and ESSs

By solving the proposed MILP model, the total cost of OSSM is obtained 2904.26$ and 3027.85$, for actual and predicted WUs generation, respectively showing less than 5% error. Considering the actual data for wind speed, Fig. 7 visualizes the day-ahead scheduling for DGs and ESSs, detailing their generation and charging and discharging activities over a 24-hour time period. Fig. 7 also highlights the dynamic operation of DGs producing energy, with separate lines indicating the output power of different DGs. Additionally, the ESSs' charging (positive values) and discharging (negative values) patterns are depicted by bar charts, showing how energy is stored and utilized throughout the day to meet electric demand. According to Fig. 7, the ESSs primarily charges between t=1 and t=8 in the early morning, which is logical given that demand during this time is lower compared to the rest of the day, while the generation of WUs is considerable during this time period. Conversely, from t=11 to t=14, which marks the first peak demand period, the ESS discharges energy to the MG. The second peak in demand, occurring between t=19 and t=22, is met through the discharge of ESSs alongside the generation from DG1, DG2, and DG3. By analogy, the OSSM taking into account the forecasted wind speed data, is depicted in Fig. 8, showing a slight deviation from Fig. 7. In other words, the difference in renewable generation between these two cases leads to a variation in scheduling, ensuring power balance while only marginally affecting the total cost of the MGs due to the precision of forecasting results.

B. Power Loss and Voltage Deviation

In the previous section, it is shown how utilizing RFR for renewable generation forecast can help MGs operator to solve OSSM indicating small error due to the small difference between actual and forecasted data. In this section, the effects of the forecast error on two crucial MG performance metrics, which are PL and VD are analyzed. The total amount of PL is obtained 428.29 kWh and 422.18 kWh for actual and forecasted scenarios, showing that the difference is less than 2% error. Similarly, total VD is achieved 10.65 and 9.53 for actual and forecasted scenarios, indicating around 1% error. The hourly PL and VD for the actual wind power generation and forecasted one are depicted in Fig. 9 and Fig. 10.

IV. CONCLUSION

The transition towards sustainable energy systems necessitates the development and integration of clean energy into microgrids (MGs). However, the inherent variability of renewable energy sources, such as wind power, pose significant challenges to the stable operation and optimization of MGs. Therefore, in this research, the potential of integrating machine learning techniques, particularly the use of a random forest regressor (RFR), in the forecasting of wind speed for wind power generation within standalone MGs is analyzed. The application of RFR in real-world, open-access wind speed data from Nottingham has not only validated the accuracy of renewable generation forecasts but has also underscored the effectiveness of these forecasts in optimizing the operation of MGs. The developed mixed-integer linear programming model for the optimal scheduling of standalone microgrids indicated that discrepancies between actual and forecasted data in terms of total cost, voltage deviation, and power loss are minimal, with errors less than 5%, 1%, and 2%, respectively. These findings highlighted the crucial role of accurate renewable generation forecasts in enhancing the operational efficiency and reliability of MGs. The suggested method has primarily been applied to predict renewable energy generation in standalone MGs. However, its applicability is not limited to this use case and the model can also forecast demand and, when MGs are connected to the grid, electricity prices. In future studies, the model will be enhanced to explore potential correlations among demand, electricity prices, and renewable energy generation in MGs.

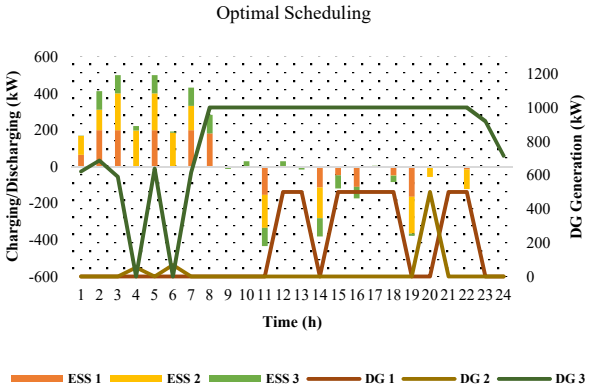

Fig. 7. Optimal scheduling of standalone MG using actual data

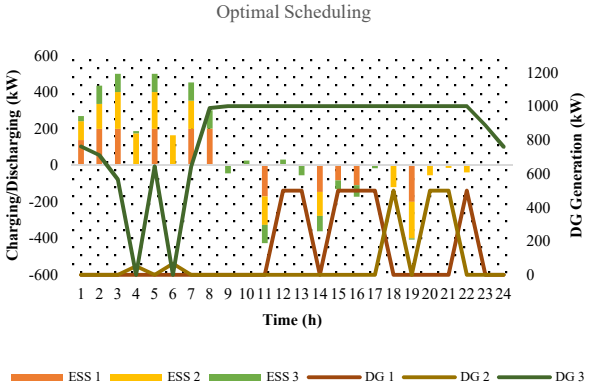

Fig. 8. Optimal scheduling of standalone MG using predicted data

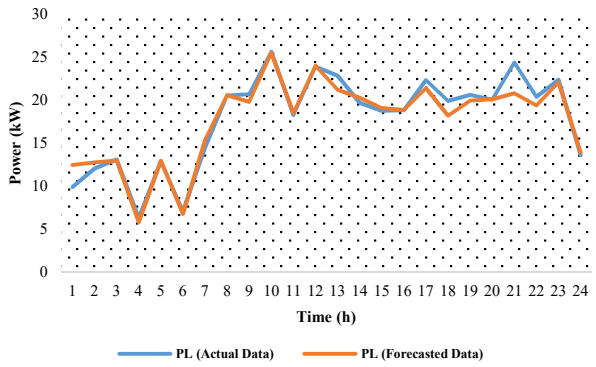

Fig. 9. Hourly power loss for actual and forecasted data

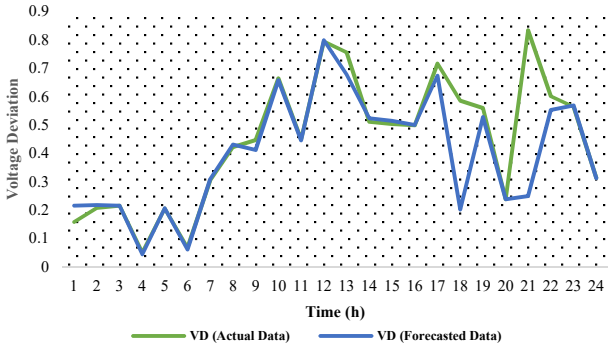

Fig. 10. Hourly voltage deviation index for actual and forecasted data

REFERENCES

[1] M. Ram et al., "Global energy transition to 100% renewables by 2050: Not fiction, but much needed impetus for developing economies to leapfrog into a sustainable future," Energy, vol. 246, p. 123419, 2022.

[2] Y. Parag and M. Ainspan, "Sustainable microgrids: Economic, environmental and social costs and benefits of microgrid deployment," Energy Sustain. Dev., vol. 52, pp. 72–81, 2019.

[3] S. F. Zandrazavi, C. P. Guzman, A. T. Pozos, J. Quiros-Tortos, and J. F. Franco, "Stochastic multi-objective optimal energy management of grid-connected unbalanced microgrids with renewable energy generation and plug-in electric vehicles," Energy, vol. 241, p. 122884, 2022.

[4] M. Mohamed, F. E. Mahmood, M. A. Abd, A. Chandra, and B. Singh, "Dynamic Forecasting of Solar Energy Microgrid Systems Using Feature Engineering," IEEE Trans. Ind. Appl., vol. 58, no. 6, pp. 7857–7869, 2022.

[5] A. Entezari, A. Aslani, R. Zahedi, and Y. Noorollahi, "Artificial intelligence and machine learning in energy systems: A bibliographic perspective," Energy Strateg. Rev., vol. 45, p. 101017, 2023.

[6] R. Wazirali, E. Yaghoubi, M. S. S. Abujazar, R. Ahmad, and A. H. Vakili, "State-of-the-art review on energy and load forecasting in microgrids using artificial neural networks, machine learning, and deep learning techniques," Electr. power Syst. Res., vol. 225, p. 109792, 2023.

[7] S. A. Shirmardi, M. Joorabian, and H. Barati, "Flexible-reliable operation of green microgrids including sources and energy storage-based active loads considering ANFIS-based data forecasting method," Electr. Power Syst. Res., vol. 210, p. 108107, 2022.

[8] B. H. Vu and I.-Y. Chung, "Optimal generation scheduling and operating reserve management for PV generation using RNN-based forecasting models for stand-alone microgrids," Renew. Energy, vol. 195, pp. 1137–1154, 2022.

[9] W. Dong et al., "Stochastic optimal scheduling strategy for a campus-isolated microgrid energy management system considering dependencies," Energy Convers. Manag., vol. 292, p. 117341, 2023.

[10] Z. Cheng, D. Jia, Z. Li, J. Si, and S. Xu, "Multi-time scale dynamic robust optimal scheduling of CCHP microgrid based on rolling optimization," Int. J. Electr. Power Energy Syst., vol. 139, p. 107957, 2022.

[11] "Ensemble methods." [Online]. Available: https://scikit-learn.org/0.16/modules/ensemble.html.

[12] P. S. Foundation, "About Python," 2024. [Online]. Available: https://www.python.org/about/.

[13] S. Developers, "Scikit-learn Tutorials," 2024. [Online]. Available: https://scikit-learn.org/stable/tutorial/index.html.

[14] S. F. Zandrazavi, A. Tabares Pozos, and J. F. Franco, "Data Clustering Method for Probabilistic Power Flow in Microgrids," in Handbook of Smart Energy Systems, Springer, 2023, pp. 1133–1154.

[15] "GE General Electric GE 1.5sl - 1,50 MW - Wind turbine," 2024. [Online]. Available: https://en.wind-turbine-models.com/turbines/20-ge-general-electric-ge-1.5sl.

[16] S. F. Zandrazavi, A. Tabares, J. F. Franco, M. Shafie-Khah, J. Soares, and Z. Vale, "A New Hybrid Fuzzy-Stochastic Model for Day-ahead Scheduling of Isolated Microgrids," in 2023 IEEE Power & Energy Society General Meeting (PESGM), 2023, pp. 1–5.

[17] S. Shubham, "zEPHYR - Wind Speed - Nottingham," 2023. [Online]. Available: https://doi.org/10.5281/zenodo.8297571.

[18] A. O. Inc., "AMPL Integrated Development Environment (IDE)," 2024. [Online]. Available: https://ampl.com/products/ampl/ide/.

[19] A. O. Inc., "AMPL CPLEX Solver," 2024. [Online]. Available: https://ampl.com/products/solvers/solvers-we-sell/cplex/.

[20] O. D. Montoya, A. Garces, and W. Gil-González, "Minimization of the distribution operating costs with D-STATCOMS: A mixed-integer conic model," Electr. Power Syst. Res., vol. 212, p. 108346, 2022.